Contact mode high-speed AFM of phase separated lipid bilayers to study Amyloid-β interactions

Morgan Robinson[1,3,4], Oliver Payton[5], Loren Picco[5], Michael Beazely[4], Mervyn Miles[5], Zoya Leonenko[1,2,3]

Affiliations:
Department of Biology[1], Department of Physics and Astronomy[2], Waterloo institute for Nanotechnology[3], School of Pharmacy[4], University of Waterloo, Waterloo, Ontario, Canada.

H.H. Wills Physics Laboratory[5], University of Bristol, Bristol, United Kingdom.

Keywords:
Atomic Force Microscopy (AFM), High-Speed AFM, Lipid bilayers, Alzheimer's disease, Amyloid-β.

Abstract

The lipid bilayer membrane is an essential feature of life, the composition and structure of which is important in governing cellular processes, some of which are mediated by the changes induced by proteins. Of particular interest is the role that the lipid membrane plays in amyloidogenic diseases such as Alzheimer's disease (AD), including the role of lipid composition and cholesterol in mediating amyloid-β (Aβ) toxicity. Atomic force microscopy (AFM) is a key tool in studying the structures of lipid membranes as nanoscale structure is important for function, unfortunately many of these dynamic processes occur on time scales where traditional AFM cannot operate fast enough. Recent advances in contact mode high-speed AFM (HS-AFM) have made it possible to capture processes at video rate. We used a unique custom-built contact mode HS-AFM to image model lipid membranes in liquid and compare this to standard and HS-AFM images. We demonstrate that this technique can be used to capture the dynamics of interactions of Aβ(1-42) monomers and oligomers with phase separated lipid bilayers composed of three and five lipid components to elucidate the role of nanoscale domains in amyloid-membrane interactions. Overall, we demonstrate the potential of the HS-AFM to image biological processes on biologically relevant soft samples and discuss tip-sample interactions at high-speed operation in contact mode on lipid membrane models in liquid environment.

Introduction

The cell membrane is the critical interface in biology which serves not only to define the extent of the cell, but also serves to compartmentalize communication and interaction both within the cell and between the cell and the environment. Lipid membrane dysfunction has been implicated in a variety of amyloidogenic diseases, including Alzheimer's disease(AD), where Amyloid-β (Aβ) has been shown to damage membrane structure which compromises the integrity of the cell, causes toxicity, disrupts ionic homeostasis and interferes with important membrane proteins which are important for receptor signaling pathways and neuron signaling [1–6]. In addition, the lipid bilayer is directly involved in non-specific interactions that are important for physiological processes including: changes in lipid membrane composition (enrichment with cholesterol, phospholipids and polyunsaturated fatty acids), interactions of small molecules and the non-specific binding of peptides and proteins[7–9]. We have previously demonstrated that changes in lipid composition directly affect amyloid-membrane interactions and amyloid-induced damage in model lipid membranes, which mimic neuronal cellular membranes in health and AD[10,11]. Thus, strategies to protect the membrane against amyloid damage by modifying membrane properties may be a feasible strategy to prevent, slow, or reverse Alzheimer's disease. This includes protective effects of small membrane active molecules such as melatonin, trehalose disaccharides as well as modifying the membrane lipid composition[10,12–14].

Atomic force microscopy (AFM) is the essential tool in nanoscience especially for analysis of biological samples that requires nanoscale spatial precision. However, traditionally it is limited by low imaging rates – on the order of minutes – therefore dynamic process cannot be imaged[15,16]. AFM generates topographical images by means of mechanical interaction with the surface. Forces between an atomically sharp probe and the sample surface cause a proportional bending of a micrometer-sized cantilever upon which the tip is attached. In contact mode, maintenance of constant tip-sample interaction forces by adjusting the height of the tip relative to the sample as the probe scans over the surface generates a topographical map of the sample. A contact mode HS-AFM system has been invented that can produce images at video rates, this not only allows for capturing dynamic changes in topography but also to generate large scale topographical images with extremely high spatial resolution within reasonably short time periods[17,18]. Previously this HS-AFM technology has been shown to be used for imaging biological samples and capturing processes despite high contact forces with the surface, for

instance collagen[19], DNA in ambient and liquid conditions[20], as well as the dissolution of tooth enamel from citric acid, [21], and more recently viral fusion on supported lipid bilayers[22]. The contact mode HS-AFM used in this manuscript differs substantially from other high speed AFM systems first pioneered by Ando et al. that operate using high-speed tapping mode, and specialized ultra-short, high resonant frequency (450-650 KHz in water), low spring constant levers[23,24]. The Ando system tapping-mode HS-AFM technology has been used previously to study amyloid aggregation on mice surfaces[25], amyloid antibody interactions[26], as well as lipid membrane interactions with carbon nanotubes[27], amyloid and antimicrobial peptides[28,29].

In this report, we show that lipid membranes and amyloid-lipid membrane interactions can be resolved at high resolution using contact mode HS-AFM. This is quite amazing considering the high contact and shear forces generated by the contact-mode HS-AFM and point to the promise of newer HS-AFM systems which utilize laser doppler feedback detection for more accurate determination of sub-nanometre height features. We also characterize the interactions between different physiologically relevant Aβ(1-42) species of differing aggregation states (monomeric vs oligomeric) on complex model lipid membranes containing high and low cholesterol. We find that monomeric Aβ(1-42) binds preferentially on liquid ordered domains, generating stable multilayer structures over several hours of incubation. In contrast, preformed Aβ(1-42) oligomers were found to bind less preferentially to the ordered domains, penetrated deeper into the bilayer, forming patches of disrupted membrane, and was prone to solubilizing and removing lipid membrane regions, generating holes in the surface. These mechanisms of interaction help to explain the relatively greater toxicity that has been associated with Aβ(1-42) toxicity and help to reveal further mechanisms of AD and provide a platform for testing therapeutics for protection of the cell membrane[30].

Methods and Materials

Contact Mode Standard AFM and Contact Mode High-Speed AFM

A modified version of a previously described HS-AFM system[18,20] was constructed in-house and mounted onto a Dimension 3100 AFM (Digital Instruments/Veeco/Bruker) which allows for standard and HS-AFM operation, see **Figure 1A** and **1B**. MLCT cantilevers with nominal spring constants of 0.01 N/m purchased from Bruker were used in all cases for both

standard and HS-AFM contact mode imaging. The HS-AFM was built using a custom stage scanner with dual sets of flexure bars driven by piezoelectric actuators in both the fast (x) and slow (y) scan directions to generate motion in the x-y plane with the applied voltages defining the scan window size, and the frequency parameters set according to the desired frame rate (Figure 1A and 1B). The window scan size was calibrated by moving the Dimension piezo tube a known distance in the x and y directions while tracking a prominent feature on the AFM movie. The cantilever was mounted onto the Dimension scan tube set to move in a 1 × 1 nm at 1 Hz line rate effectively providing negligible motion in the x-y plane while still allowing the scan tube to provide control over the z movement using the Dimension feedback and controller system (Nanoscope V4, NanoScope IIIa or NanoScope IV Controller – Digital Instruments). A constant cantilever deflection was maintained by the Dimension feedback loop set at 1 nN. The HS-AFM controller (written in-house using LabVIEW) applies a sinusoidal voltage to drive the scan stage, both fast and slow scan axes with the frequency parameters set according to the desired frame rate. In-house written data collection software takes the magnitude of the cantilever bending from the Dimension 3100 photodiode via the NanoScope Signal Access Module (Digital Instruments) as the stationary probe sits in contact with the surface via the standard optical lever method – data is then linearized to account for the sinusoidal motion of the scan stage.

Complex biomimetic supported lipid bilayers

Two model lipid membranes were used in this work: 3-component membrane composed of DPPC/DOPC/Chol at low (45:45:10 by weight) and high cholesterol (40:40:20 by weight) concentration and 5-component membrane composed of DPPC/POPC/Chol/sphingomyelin/GM1 (39:39:10:10:2)[10]. DPPC, 1-palmitoyl-2-oleoyl-sn-glycero-3-phosphocholine (POPC) purchased from Sigma Aldrich, Cholesterol purchased from Avanti Polar Lipids, and Sphingomyelin and GM1 (monosialotetrahexosylganglioside) sodium salt from bovine brain purchased from Santa Cruz Biotechnology. Supported lipid bilayers were produced by vesicle fusion (Figure1C), briefly: each lipid was dissolved in chloroform at a concentration of 1 mg/ml mixed at various ratios then evaporated under dry N_2 gas. Complex lipid mixtures in chloroform were left overnight to evaporate producing a multilamellar thin film of mixed lipid layers. The thin films were then suspended in ultrapure water to 0.5 mg/ml and a SUV solution for vesicle fusion was produced using the sonication method. Vesicle solutions were made one day prior to use, stored in the fridge overnight and then run through 4-8 cycles of 15 min sonication followed by 15 min

of stirring immediately prior to vesicle fusion onto freshly cleaved mica substrates, until solutions turned from cloudy to translucent. SUV solution (100 μL) on mica was then incubated on the sample for 2 hours to establish a stable supported lipid bilayer, before being washed 5 times with MilliQ water (>18.2 MΩ) by exchange 100 μL of solution in the liquid droplet.

Monomeric and Oligomeric Amyloid-β Preparation

Aβ(1-42) ultrapure, HFIP treated, (rPeptide) was prepared in monomeric and oligomeric form following protocols previously described[31]. Briefly, dry 1mg Aβ film was suspended in HFIP (Millipore-Sigma) to a concentration of 1mg/mL, aliquots of 0.1mg were prepared by pipetting 100μL into 1.5mL centrifuge tubes, placed in desiccated environment under vacuum overnight. The next day aliquots were placed in -20°C until ready for preparation. Monomeric Aβ was prepared by first making 5 mM solution in DMSO, scraping the sides of the tube and sonicating for 20 minutes in cold water bath. Next, ice-cold MilliQ water was added to the tube and kept on ice. For treatment of supported lipid bilayers, monomeric Aβ was used immediately being injected at 20 μL into the 180 μL liquid droplet for a final concentration of 10 μM. Aβ oligomers were incubated overnight at 4°C overnight, at least 18 hours at 100 μM in ultrapure water before being injected into the liquid cell, also at a final concentration of 10 μM. Aβ was injected into the liquid droplet during scanning for some experiments or was incubated on the supported lipid bilayer for 1 hour, before washing 2 times with 100 uL MilliQ water, prior to being imaged. Aβ Fibrils were prepared by incubation overnight in 50 μM HCl solution at 37°C overnight as a positive control to validate amyloidogenic capacity.

Image acquisition and processing and analysis

For all imaging, the lipid membranes were supported on mica and imaged in water in liquid AFM cell. The standard contact mode images shown herein were acquired using the standard Dimension 3100, with Nanoscope 4 (NanoScope Software version 4). Images were sampled using 512 × 512 px image settings at a line scan rate of 0.5 – 1 Hz, with feedback set below 1 nN of force. Images were then exported into Gwyddion software, plane leveled, Gaussian filter of 3 px applied. For cross section analysis 5px line width was used. Roughness parameters were calculated by measuring the RMS roughness of each cross section.

For HS-AFM images, in-house LabView Software was used to send, receive and process signals for driving the high-speed scan stage. The frame rate was set to 1 Hz, with 1000 Hz fast

scan and 1 Hz in slow scan direction. Electronic phases were manually adjusted to allow for adequate x-y mapping of the Z-deflection signals. The size of the scan window was manually adjusted by the use of a Sony Amplifier. Data was linearized to account for approximate sinusoidal motion of the scan stage. HS-AFM videos were then exported from LabVIEW into AVI files and then frames were extracted into image sequences using OpenCV packages in python. Individual frames were then imported into Gwyddion, plane leveled, Gaussian filter of 3 px applied, for cross section analysis 5px line width was used, and roughness parameters were calculated by measuring the RMS roughness of each cross section.

Results and Discussion

Contact mode HS-AFM of supported lipid bilayers

The contact-mode HS-AFM system was developed in-house by modification of the Dimension 3100 AFM instrument (**Figure 1A, B**). Calibration of HS-AFM XY scale can be done in two ways; the first is to directly compare identical features under standard and high-speed operation provided a standard AFM image is taken before. Alternatively, under high-speed operation the scan tube can be translated by a set distance across the surface, the resulting translation can be seen and measured by tracking features on the HS-AFM. There are small discrepancies between measuring distances in this way as compared to the x-y scale generated from the Dimension under standard operation. Calibration of the z scale using this modified Dimension 3100 HS-AFM system is less trivial, since the HS-AFM image is generated by plotting the deflection signals directly. The output of the deflection signals from the Dimension piezo tube are calibrated by the Dimension software using a calibration grid, however the native Dimension software does not communicate to the HS-AFM software directly and therefore raw Z-deflections signals cannot be scaled by the HS-AFM software. For the work presented in this report, the HS-AFM system does not have a feedback system with which to calibrate the scale. One way to generate a z-scale is to compare two identical features captured under standard and high-speed operation and calibrate them. Otherwise force curves on the samples can be taken to calibrate the cantilever sensitivity and provide an estimate of the bending angle per unit of voltage on the photodiode detector signal. This limitation of estimating the sample surface heights is not an issue on new HS-AFM systems that have recently been developed that use a

laser Doppler vibrometer as that detection system is able to directly monitor the vertical displacement (z height) of the cantilever tip from the sample surface[22,32].

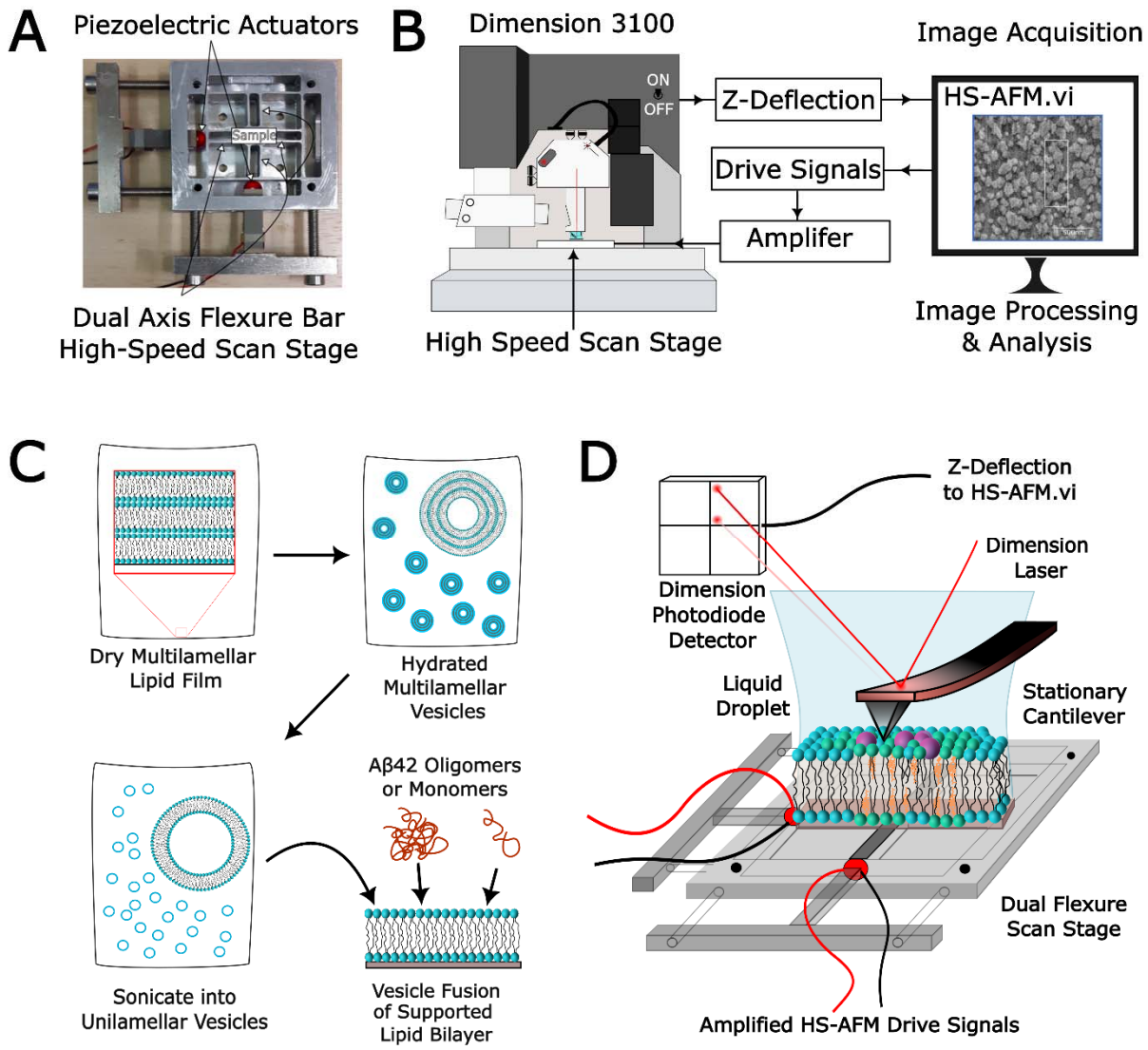

Figure 1. (**A**) HS-AFM dual axis flexure scan stage. (**B**) In-house HS-AFM system integrated with a Dimension 3100 AFM. Sinusoidal AC voltage drive signals are applied to the scan stage piezoelectric actuators from the HS-AFM controller. The amplitude of the sin waves determines the frame/image size, while the frequency governs the frame rate. The Dimension 3100 scan tube is set stationary (1nm x 1nm scan window size), and the feedback setpoints are set to maintain surface contact with an average force, below 1nN, cantilever deflection signal is sent to HS-AFM drive and analysis software through a Bruker Breakout Box and plotted in real-time during scanning. (**C**) Supported Lipid Bilayer was produced by sonication and vesicle fusion onto freshly cleaved mica. (**D**) Schematic representation of the lipid bilayer being imaged on the HS-AFM scan stage.

Complex lipid mixtures are often used to study the organization and biophysical properties of lipid membranes that possess micro- and nano-domains, typically model membranes composed of 3 or more lipids are considered complex. A side-by-side comparison of AFM and HS-AFM images of a complex neuronal model membrane composed of 5 different lipid species was used and shown in Figure 1; it is composed of: DPPC (36.5% by mole), POPC (35.2 % by mole), cholesterol (17.8 % by mole), sphingomyelin (9.7% by mole) and gangliosides GM1 (0.09% by mole). This complex model lipid system was used previously as biomimetic Alzheimer's disease (AD) model membrane (Diseased Membrane 1 – DM1) and was shown to be rendered more susceptible to Aβ damage[10], and be protected from Aβ-induced damage by melatonin[13]. Standard AFM images of one of these model membranes are shown below along with a HS-AFM image of the same membrane and same region in Figure 2. It appears there is a minor x-y distortion of the HS-AFM image when comparing it to the standard AFM, that cannot be corrected by simple linearization of the sinusoidal drive signals. It appears as though there is compression along the fast scan axis (image below fast scan is in the y-direction, which caused by Piezo hysteresis which can be corrected by additional optical interferometry of the scan stage position at higher costs[32]. In addition, we observed some minor clockwise skewing of the image which is due to imperfections in the perpendicularity of the slow and fast scan axis piezos, which are not perfectly aligned 90 degrees to one another. Although the tip trajectory over the scan can mostly be accounted for these two simple linear transformations, additional motion of the cantilever tip in the z direction needs to be corrected to better map standard AFM images to the HS-AFM frames. Regardless of this minor x-y distortion HS-AFM imaging resolution is comparable to standard AFM. Though there appears to be greater overall image noise, as shown by the cross section in **Figure 2C** and **2D**. This is variable and depends on tip and sample quality.

Two major advantages of HS-AFM imaging were apparent in our study. First, that HS-AFM imaging allows for rapid assessment of sample quality, within one or two frames of imaging it can be determined whether a good lipid bilayer is formed, then a rapid assessment of large-scale sample homogeneity can be determined within only a matter of 1 or 2 minutes, thus making troubleshooting poor sample preparation very effective. This is a process that routinely takes over an hour or longer for standard AFM. Secondly, there are less line-to-line mismatch aberrations, and horizontal scarring type AFM artefacts, which allow more of the data to be of

high quality and keeps image processing time down. We observed large differences in sample integrity between samples deposited from the same stock solution of lipid vesicles. This points to small differences in ambient conditions, mica surface quality, and lipid stability in solution as difficult to control factors in supported lipid bilayer quality.

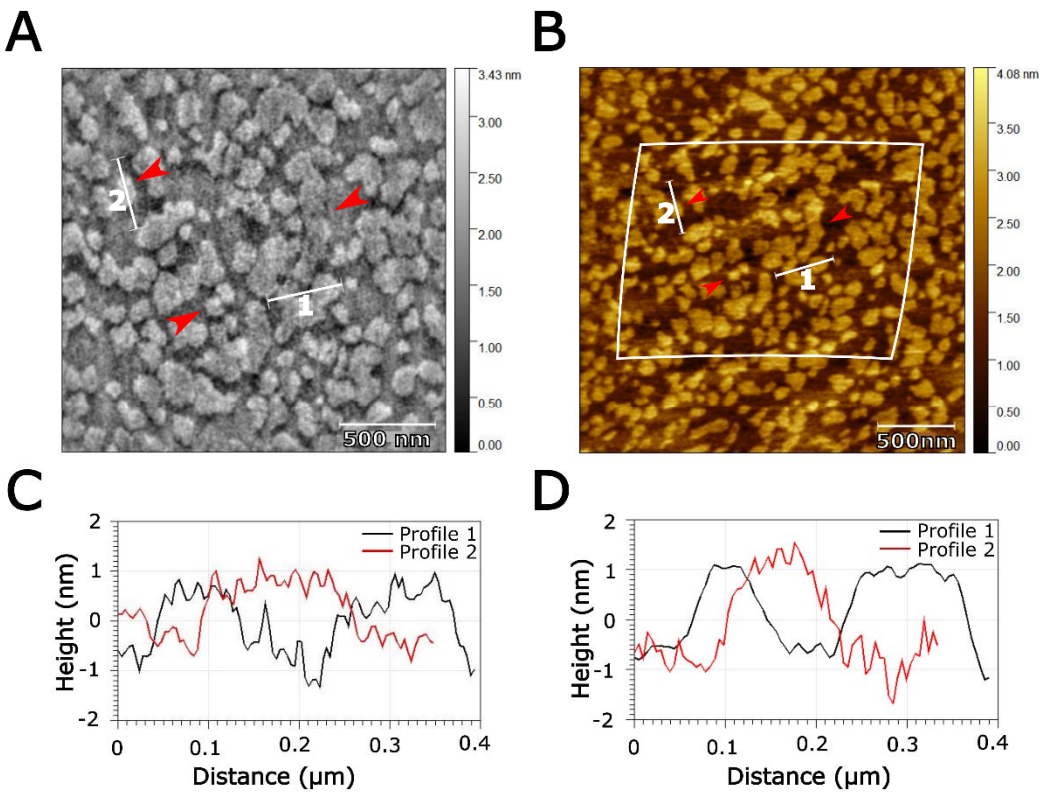

Figure 2. Side by side comparison of (**A**) HS-AFM (2µm×2µm) and (**B**) standard AFM showing the outline of the HS-AFM scan window (2.5µm×2.5µm). Red arrows and cross sections are matched across the two different imaging modalities. HS-AFM scale and vertical axis was calibrated from the standard AFM imag extents. (**C**) and (**D**) Cross-section profiles are indicated on the standard and HS-AFM image across L_O domains, corresponding to cholesterol, sphingomyelin and ganglioside enriched nanodomains.

The effect of Aβ(1-42) on 3 component DOPC/DPPC/Chol membranes.

In this part of the study two different phase separated lipid bilayer models were used to study the effects of different aggregation states of Aβ (monomer and oligomer), on interactions with cholesterol containing mammalian supported lipid bilayers. Here membrane vesicles were formed and then allowed to self-assemble into supported lipid bilayers where control images were taken with the HS-AFM system. These lipid bilayers were then treated with 10 µM Aβ (either monomer or oligomer) for 1 hour before being rinsed and then imaged again. Sample homogeneity across very large ~ 2 - 4 mm^2 areas were determined by manual moving the scan

stage with the course adjust, samples with high heterogeneity were discarded, for example: incomplete surface coverage, large holes, or large differences in membrane structure. For data collection, the HS-AFM scan window size was set to ~3.5 x 3.5 µm before the scan window was moved in a raster pattern across 10 steps in each x and y direction (for 100 frames). The raster step size was 2 µm and 3 different regions, 2-3 mm distant from one another, were measured for each sample. Aβ was added to the membrane sample, incubated for 60 minutes to allow lipid membrane-amyloid complexes to form, and then excess of amyloid in the bath was washed away prior to imaging.

Representative control DOPC/DPPC/Cholesterol containing lipid bilayers at 40:40:20 (high cholesterol content) and 45:45:10 (low cholesterol content) by weight (or approximately 1:1:1 and 2:2:1 by molar ratio), are shown in Figure 3 along with their respective cross-sections are shown, Height profiles between domains were between 0.7 and 1.0 nm for both membranes, similar to what is expected based on previous studies[33,34]. These height differences correspond to the two distinct phases of these membranes, the disordered phase enriched in unsaturated phospholipids, and the ordered phase – enriched in cholesterol and unsaturated lipids. Membranes with lower cholesterol concentration (2:2:1), tended to have more narrow domains that were interconnected across large scan areas, whereas high cholesterol membranes tended to have more isolated domains. Although this effect was variable, and likely depends on fluctuations in ambient temperature and small variations in lipid ratios from sample to sample, as these models lay very close to the phase boundaries for these particular samples[33]. Variability in lipid membrane domain structure prior to Aβ treatment was observed due to changes in ambient conditions temperature, humidity and small differences in stoichiometry of the lipids, and lipid stability.

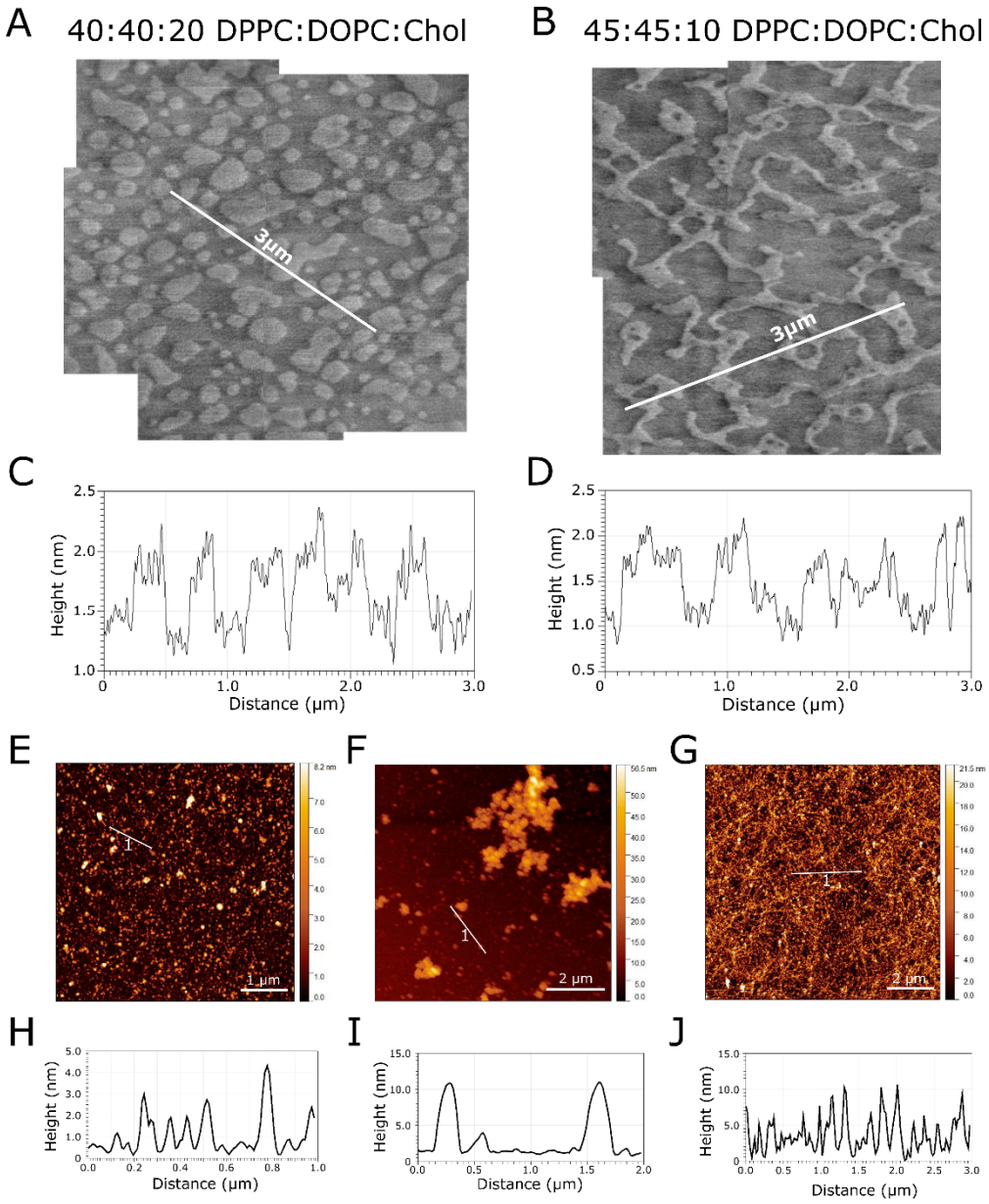

Figure 3. (A) and **(B)** The structure of DOPC/DPPC/Cholesterol lipid bilayers at different molar ratios of 1:1:1 and 2:2:1 with cross sections displayed in **(C)** and **(D). (E)**, **(F)** and **(G)** show representative control images of monomers, oligomers and fibrils on mica substrate, along with the respective cross sections in **(H)**, **(I)**, and **(J).**

After acquiring control images of the membrane models, Aβ as monomers or pre-aggregated oligomers were added to the liquid droplet, incubated, washed and then imaged. Representative monomeric and oligomeric Aβ(1-42) AFM images of monomers and oligomers are shown in Figure 3E and 3F, along with a control experiment to show that the Aβ preparations are capable of fibrilization (Figure 3G). Cross-sections Aβ show monomers varied in size from >0.5 nm to 4 nm, monomers are likely undergoing some aggregation during their deposition on

mica, while oligomers were much larger ranging from 5 - 25 nm in diameter. It is observed that as the HS-AFM scan window moves to a new scan region containing Aβ aggregates on the surface, some of these taller aggregates can be swept off or possibly pressed into the lipid bilayer by the AFM probe. This could be due to differences in binding affinity of the taller aggregates on the surface or due to greater shear forces at larger heights from the AFM probe as it scans over taller image features on the surface. This leaves behind stable aggregates that are more strongly bound to the ordered domain lipid bilayer surface which are stable under high-speed scanning for at least 100 s of HS-AFM frames .

In low concentration cholesterol membranes treated with Aβ prepared in monomeric form Aβ monomers bind preferentially to the ordered membrane microdomains, taller domains, producing structures that protruded above the lower disordered membrane phase by 1.8 ± 0.3 nm after 2 hours and 2.2 ± 0.2 nm after 8 hours. Aβ incubation for 2 hours on lipid bilayers produced less tightly bound Aβ aggregates on the surface (**Figure 4A** and **4D**). After 8 hours, Aβ monomer and lipids appear to organize into very stable multi-layered domains, of 0.9 and 2.2 nm above the disordered lipid phase (**Figure 4B**). At the 2-hour timepoint the RMS line roughness of the Aβ region on the membrane was increased by 43 ± 18%, then after 8 hours this increased to 70 ± 16% (**Figure 4G** and **4H**). The increase in surface roughness with time is due to the increased height of Aβ aggregates on the ordered domains in the 8-hour timepoint.

Low cholesterol lipid bilayers treated with preformed oligomeric Aβ exhibited unique membrane interactions (**Figure 4C**), first the oligomers did not appear to exhibit preferential binding to the ordered membrane phases, Aβ oligomers bound to the disordered and ordered domains indiscriminately resulting in disruption to both phases of the lipid bilayer, inducing holes alongside the protruding Aβ oligomers in clusters. The height of the tallest oligomers above the disordered phase was 1.5 nm with minimum heights below the plane levelled mean, indicative of holes in the membrane (**Figure 4F**). These aggregates had increased line surface roughness over the ordered domains, by 16 ± 9 %, which was the lowest roughness among all the groups (**Figure 4I**). This is likely due to the aggregates penetrating deeper into the disordered phases of the lipid bilayer, rather than sitting atop the ordered phases.

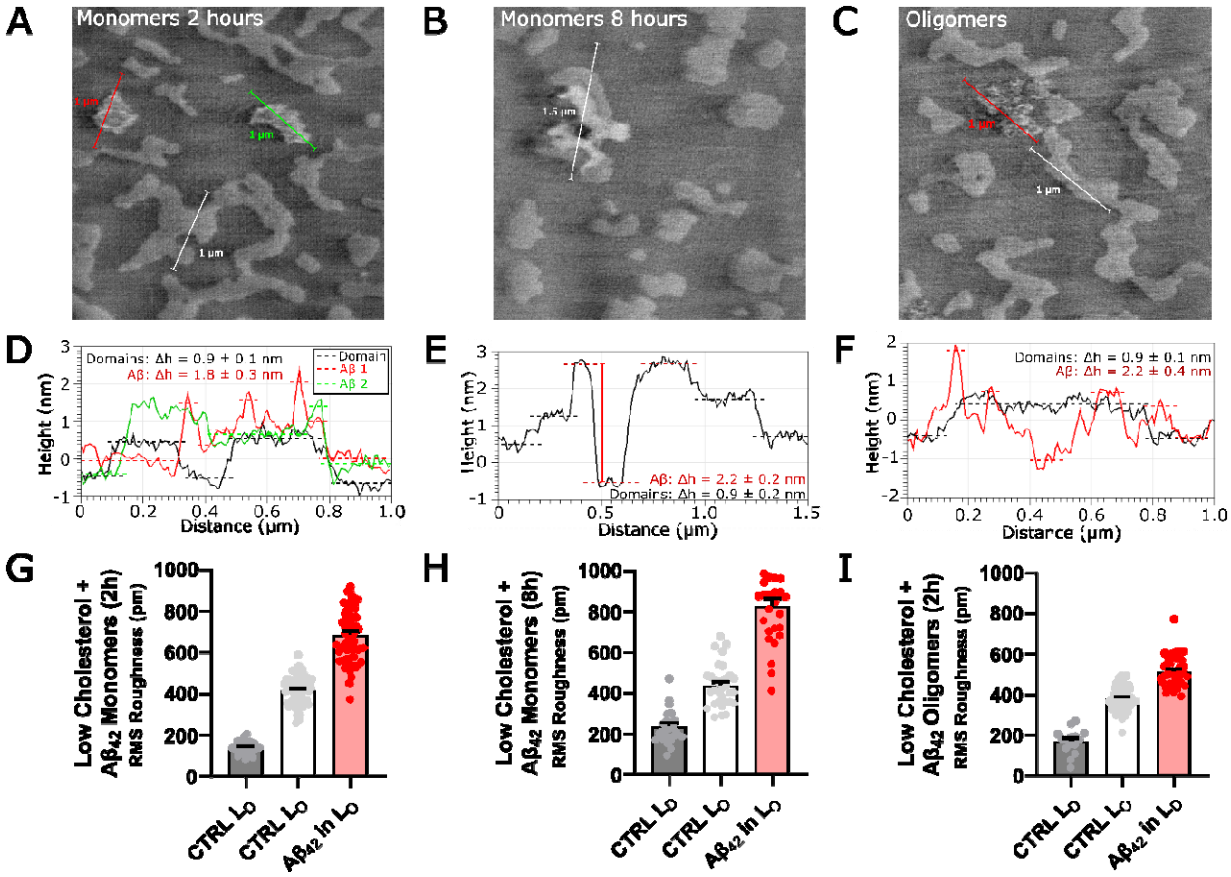

Figure 4. Low cholesterol lipid bilayers (DPPC/DOPC/Cholesterol – 45:45:10 by weight) treated with $A\beta_{42}$ for (A) 2 hours and (B) 8 hours. Aggregates preferentially bind to ordered membrane microdomains and are initially unstable, able to be swept off the surface of the lipid bilayer by HS-AFM imaging after 8 hours aggregates form stable multilayers on ordered domains. (C) Low cholesterol lipid bilayer treated with preformed Aβ oligomers. Corresponding Cross-sections are shown below each representative image (D), (E) and (F). (G), (H) and (I) Increase in membrane surface roughness is observed in regions where Aβ monomers and oligomers have bound to and disrupted membrane topography, RMS roughness of the flat Liquid Disordered domains is shown to illustrate background RMS roughness. Each dot represents a cross section from one frame, repeated across several different areas and samples.

We observed several different morphologies of Aβ monomers on high cholesterol containing membranes, again it was observed that Aβ monomers bind to ordered membrane domains, which are most apparent at the boundaries of the domains (**Figure 5A**). We also observe small pore-like structures, which could form as monomers accumulate at the boundary of a small, ordered domain (**Figure 5B**). A more detailed frame-by-frame analysis of the pore-like structure reveals 4 to 5 globular aggregates arranged in a ring. This similar morphology of amyloid ion channels was detected previously, though in that model system the lipid-Aβ preparation was made in proteoliposome deposition, where Aβ was mixed with the lipids in organic solvent, left to evaporate and produce a thin film and then resuspended into a supported lipid bilayer[35]. This proteoliposome system is much less physiologically relevant than the

protocol used here, as Aβ is expected to deposit onto cell membranes from the extracellular space. Ordered domain heights are approximately 0.9 ± 0.1 nm above the disordered phase with Aβ monomers protruding to 1.8 ± 0.3 nm above the disordered phase, for this Aβ-lipid membrane complex. Aβ aggregates on the lipid membrane surface increased membrane surface RMS roughness by 63 ± 15% (**Figure 5I**).

High cholesterol lipid bilayers exposed to Aβ oligomers also exhibited more obvious damage to the lipid bilayers in the form of holes more than monomeric Aβ, as in the case of low cholesterol membranes (**Figure 5E** and **5F**). There are two different types of interaction mechanisms observed for Aβ oligomers with high cholesterol membranes. First, binding and aggregation onto the ordered domains like in the case of monomers sitting about 1.8 nm above the membrane surface (**Figure 5G**). Second, there was also a distinct formation of large and deep holes in the membrane, penetrating as much as 2.1 nm below the ordered phase (**Figure 5H**). This type of extraction of the lipids from the membrane surface by amyloid is likely due to some solubilization-like effects that have been reported previously[36]. Typically, bilayer thickness is reported to be at minimum 5 nm, therefore the 2.1 nm depth of the hole could be indicating removal of only the top leaflet or could be a result of tip convolution effects. Regardless, the damage to the membrane is apparent, and distinct compared to all other conditions tested here. Surface roughness analysis does not reveal a difference between the two conditions at 41 ± 17% and 40 ± 2 % RMS surface roughness over the ordered domain to the amyloid containing domain (**Figure 5J** and **5K**).

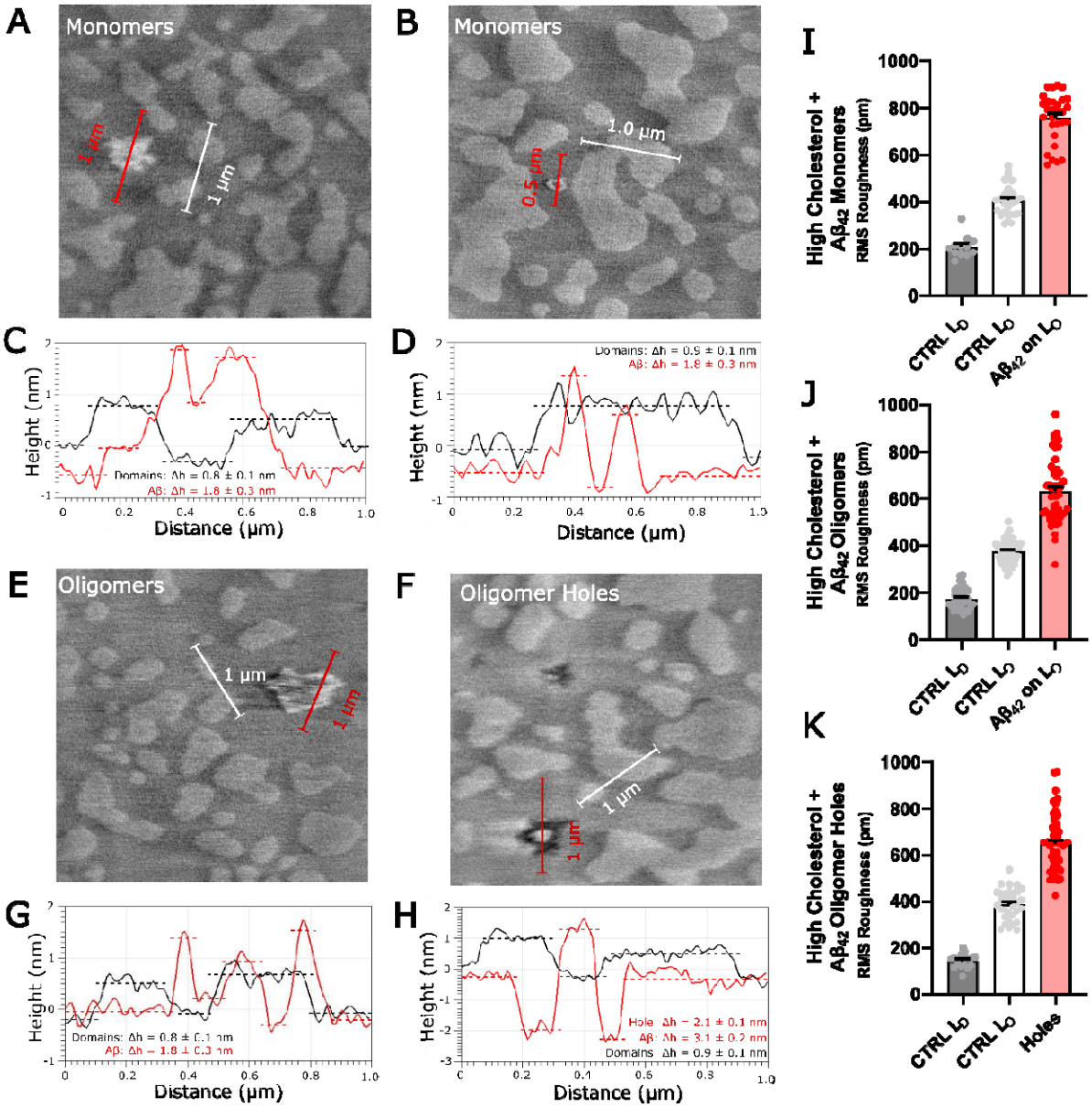

Figure 5. High cholesterol (DPPC/DOPC/Cholesterol – 40:40:20 by weight) membranes treated with Aβ Monomers (A)-(D) and preformed Aβ oligomers (E)-(H), and roughness analysis (I)-(K). (A)-(D) monomeric Aβ was less disruptive to the membrane, forming more stable structures on the ordered domains, cross sections exhibit an increase in domain height over domains not occupied by Aβ. Membrane line RMS roughness for (I) High Cholesterol Bilayer treated with Aβ(1-42) monomers, (J) High Cholesterol Bilayer treated with Aβ(1-42) Oligomers and (K) High Cholesterol Bilayer Aβ(1-42) induced holes; RMS roughness of the flat Liquid Disordered domains are shown to illustrate background RMS roughness. Each dot represents a cross section from one frame, repeated across several different areas and samples.

Low and high cholesterol lipid bilayers treated with Aβ monomers and oligomers exhibit different membrane interactions with some common trends across treatment conditions. In all cases Aβ increased surface roughness, (both mean and RMS), as well as increases in height on all the AFM images. Preferential binding of Aβ monomers and oligomers to high cholesterol ordered lipid domains was observed in most cases, except for low cholesterol membranes treated

with oligomers. In both low and high cholesterol membranes Aβ monomers bound to ordered domains and formed aggregates on top of the membrane, in comparison Aβ oligomers were observed to penetrate the membrane and form holes in the lipid bilayer, and even remove membrane material. Aβ oligomers are known to be more toxic than monomers, this difference in toxicity could be due to the differences observed in this HS-AFM study, that oligomers are more likely to penetrate and form holes in the membrane, whereas monomers simply bind to the membrane surface and not able to penetrate the membrane. Although cholesterol metabolism has been implicated in AD through metabolic and genetic risk factors (most notably ApoE ε4 alleles)[37], many uncertainties remain, and controversial hypotheses for the role of cholesterol in AD pathogenesis need to be resolved. The cholesterol dependence of Aβ toxicity has been evaluated in many studies showing opposite effects, in some studies cholesterol depletion is shown to be protective[2,6], while others show that cholesterol enrichment is protective[38]. These discrepancies could be due to differences in the aggregation state of amyloid or cell types. In this study, we show that oligomers can damage both low and high cholesterol membranes but in unique ways depending on lipid membrane cholesterol composition.

Conclusion

In this report, we used a custom-built contact mode HS-AFM for studying protein-lipid bilayer interactions related to neuroscience and neurodegeneration in Alzheimer's disease. Typical AFM experiments are long and arduous to collect data, when a single high-resolution image often takes upwards of 20 minutes to gather, then process and analyze. The ability to gather images of comparable quality in the order of seconds means that projects have the potential to be sped up by several orders of magnitude. Ultra-short cantilever, high frequency tapping mode AFM is another high-speed technology capable of imaging biological membranes and was used to study Aβ interactions with biomimetic membranes composed of SM/POPC, SM/POPC/Chol and SM/POPC/Chol/GM1[28,29]. They showed that the inclusion of gangliosides was necessary for binding to the model membrane and that GM1 caused rapid dissolution of the membrane during exposure to mutant Aβ-G37C peptide oligomers[29], and that various mutations in Aβ also affected interactions with their model lipid membranes[28]. In our manuscript here, we show that amyloid can form stable aggregates on the surface of membranes composed of different levels of cholesterol and that the stability of these structures depends on the identity of

the amyloid species and the cholesterol content of the membrane itself. Both the contact-mode work presented here, and previous tapping mode HS-AFM systems are able to capture lipid-protein interactions and study the effects of membrane composition and amyloid species. The resolution of each HS-AFM is comparable, though the Ando system may outperform the resolution of the contact-mode system presented here due to the smaller tip diameter. However, our contact-mode AFM is much faster able to capture more than 1 frame/second with scan areas of 2-4 nm at 512x512 pixels[2], compared to 1 frame/second at 800x800nm reported. It is difficult to make conclusive statement regarding the advantages of each system for studying protein-lipid membrane interactions at this early stage. Overall, the results here show that it is possible to constantly image an extremely soft sample by HS-AFM to study peptide-lipid and lipid-small molecule interactions with improved temporal resolution and greater sample statistics.

Constant contact HS-AFM imaging of soft biological membranes can exhibit destructiveness to poorly fused lipid bilayers. The constant contact high speed scanning was also observed to induce some mixing of the lipid bilayer components under very long imaging times, reducing ordered domain visibility. However, nondestructive high-quality imaging of the lipid bilayer was also shown to be highly reproducible, provided sufficient bilayer fusion has occurred. Non-destructive HS-AFM imaging relies on interesting probe-sample dynamics during high-speed scanning: hydrodynamic lift-off of the probe tip and super-lubricity of the ultra-confined water structure trapped between the tip and the sample are proposed as explanations[19]. This HS-AFM is a relatively non-destructive method for imaging soft bilayers comparable image quality to standard contact AFM mode in liquid. It is possible to limit the effects of the tip over longer-term imaging by taking snapshots and not undergoing constant imaging or scanning over multiple areas spending a short period of time at each location – although these strategies would lower the time resolution of HS-AFM imaging. Newer HS-AFM systems that use laser Doppler vibrometer detection systems and do not have active feedback systems may also be superior for imaging peptide lipid interactions, as the probe height can be kept constant and the force on the surface controlled by height, rather than in feedback system which is sensitive to fluctuations in forces during scanning[22]. The ability to image dynamic membrane processes with sub-second timescales, as well as collecting several orders of magnitude more data has exciting applications.

This work extends the applications of contact mode HS-AFM to very soft lipid bilayer samples for studying protein aggregation and exploring an important question in molecular

neurodegeneration. This work contributes to the understanding of different interaction mechanisms that can occur between different amyloid-β species and lipid membranes of differing cholesterol concentration. Aβ monomers tended toward binding on top of ordered lipid membrane domains in both low and high cholesterol cases forming stable multilayers. Whereas Aβ oligomers bound to both domains and often resulted in penetration and perforation of the lipid bilayer. This may in part explain the increase in toxicity of oligomers over monomers that is often reported in the literature. There were large differences in the interaction mechanisms, as indicated by the differences in surface topography, between the different cholesterol levels and the aggregation state of Aβ. These differences are time-dependent and thus rates of molecular diffusion and proteo-lipid organization are likely important in Aβ toxicity.

Acknowledgement

We would like to acknowledge the International Strategic Partnership Grant from the University of Waterloo (awarded to Zoya Leonenko) and the Collaborative Initiative Grant from the University of Bristol (awarded to Mervyn Miles) for funding this work, as well as MITACS Globalink, the Ontario Graduate Scholarship and Waterloo Institute of Nanotechnology Nanofellowship awarded to Morgan Robinson. As well as NSERC grants awarded to Michael Beazely and Zoya Leonenko. We would also like to acknowledge Dr. Liz Drolle for discussions on complex lipid membrane preparation, Dr. Robert Richardson and Dr. Annela Seddon for use of their laboratory prep space and Mr. Ravi Sharma for assistance with data collection.

Contributions

Conceptualization and project design by Zoya Leonenko and Mervyn Miles. HS-AFM design and build by Loren Picco, Oliver Payton and Mervyn Miles. Lipid and protein protocols by Morgan Robinson, Michael A. Beazely and Zoya Leonenko; Imaging and image analysis by Morgan Robinson and Mervyn Miles; manuscript written and edited by Morgan Robinson with contributions from all authors.

Conflict of interest

The authors declare that the research was conducted in the absence of any commercial or financial relationships that could be construed as a potential conflict of interest.

References

(1) Zampagni, M.; Evangelisti, E.; Cascella, R.; Liguri, G.; Becatti, M.; Pensalfini, A.; Uberti, D.; Cenini, G.; Memo, M.; Bagnoli, S.; Nacmias, B.; Sorbi, S.; Cecchi, C. Lipid Rafts Are Primary Mediators of Amyloid Oxidative Attack on Plasma Membrane. *J. Mol. Med.* **2010**, *88* (6), 597–608. https://doi.org/10.1007/s00109-010-0603-8.

(2) Nicholson, A. M.; Ferreira, A. Increased Membrane Cholesterol Might Render Mature Hippocampal Neurons More Susceptible to Beta-Amyloid-Induced Calpain Activation and Tau Toxicity. *J. Neurosci. Off. J. Soc. Neurosci.* **2009**, *29* (14), 4640–4651. https://doi.org/10.1523/JNEUROSCI.0862-09.2009.

(3) ARISPE, N. Plasma Membrane Cholesterol Controls the Cytotoxicity of Alzheimer's Disease AbetaP (1-40) and (1-42) Peptides. *FASEB J.* **2002**, *16* (12), 1526–1536. https://doi.org/10.1096/fj.02-0829com.

(4) Cecchi, C.; Stefani, M. The Amyloid-Cell Membrane System. The Interplay between the Biophysical Features of Oligomers/Fibrils and Cell Membrane Defines Amyloid Toxicity. *Biophys. Chem.* **2013**, *182*, 30–43. https://doi.org/10.1016/j.bpc.2013.06.003.

(5) Hicks, D. A.; Nalivaeva, N. N.; Turner, A. J. Lipid Rafts and Alzheimer's Disease: Protein-Lipid Interactions and Perturbation of Signaling. *Front. Physiol.* **2012**, *3 JUN*. https://doi.org/10.3389/fphys.2012.00189.

(6) Robinson, M. J.; Newbury, S.; Singh, K.; Leonenko, Z.; Beazely, M. A. The Interplay Between Cholesterol and Amyloid-β on HT22 Cell Viability, Morphology, and Receptor Tyrosine Kinase Signaling. *J. Alzheimers Dis.* **2023**, *96* (4), 1663–1683. https://doi.org/10.3233/JAD-230753.

(7) Hane, F.; Drolle, E.; Gaikwad, R.; Faught, E.; Leonenko, Z. Amyloid-?? Aggregation on Model Lipid Membranes: An Atomic Force Microscopy Study. *J. Alzheimers Dis.* **2011**, *26* (3), 485–494. https://doi.org/10.3233/JAD-2011-102112.

(8) Pécheur, E. I.; Sainte-Marie, J.; Bienvenüe, A.; Hoekstra, D. Peptides and Membrane Fusion: Towards an Understanding of the Molecular Mechanism of Protein-Induced Fusion. *Journal of Membrane Biology*. 1999, pp 1–17. https://doi.org/10.1007/s002329900466.

(9) Drolle, E.; Ku??erka, N.; Hoopes, M. I.; Choi, Y.; Katsaras, J.; Karttunen, M.; Leonenko, Z. Effect of Melatonin and Cholesterol on the Structure of DOPC and DPPC Membranes. *Biochim. Biophys. Acta - Biomembr.* **2013**, *1828* (9), 2247–2254. https://doi.org/10.1016/j.bbamem.2013.05.015.

(10) Drolle, E.; Negoda, A.; Hammond, K.; Pavlov, E.; Leonenko, Z. Changes in Lipid Membranes May Trigger Amyloid Toxicity in Alzheimer's Disease. *PLoS ONE* **2017**, *12* (8), e0182194.

(11) Drolle, E.; Gaikwad, R. M.; Leonenko, Z. Nanoscale Electrostatic Domains in Cholesterol-Laden Lipid Membranes Create a Target for Amyloid Binding. *Biophys. J.* **2012**, *103* (4), L27–L29. https://doi.org/10.1016/j.bpj.2012.06.053.

(12) Mei, N.; Robinson, M.; Davis, J. H.; Leonenko, Z. Effect of Melatonin on Lipid Membrane Structure and Membrane Interactions with Amyloid. An NMR and LSPR Study. *Biophys. J.* **2020**, *118* (3), 385a. https://doi.org/10.1016/j.bpj.2019.11.2194.
(13) Mei, N.; Liang, J.; McRae, D. M.; Leonenko, Z. Localized Surface Plasmon Resonance and Atomic Force Microscopy Study of Model Lipid Membranes and Their Interactions with Amyloid and Melatonin. *Nanotechnology* **2024**, *35* (30), 305101.
(14) Xu, Y.; Filice, C. T.; Leonenko, Z. Protective Effect of Trehalose Sugar on Amyloid-Membrane Interactions Using BLM Electrophysiology. *Biophys. J.* **2024**, *123* (12), 1690–1704. https://doi.org/10.1016/j.bpj.2024.05.012.
(15) Binnig, G.; Quate, C. F.; Gerber, C. Atomic Force Microscope. *Phys Rev Lett* **1986**, *56* (9), 930. https://doi.org/10.1103/PhysRevLett.56.930.
(16) Drolle, E.; Hane, F.; Lee, B.; Leonenko, Z. Atomic Force Microscopy to Study Molecular Mechanisms of Amyloid Fibril Formation and Toxicity in Alzheimer's Disease. *Drug Metab. Rev.* **2014**, *46* (2), 207–223. https://doi.org/10.3109/03602532.2014.882354.
(17) Humphris, A. D. L.; Miles, M. J.; Hobbs, J. K. A Mechanical Microscope: High-Speed Atomic Force Microscopy. *Appl. Phys. Lett.* **2005**, *86* (3), 1–3. https://doi.org/10.1063/1.1855407.
(18) Payton, O. D.; Picco, L.; Miles, M. J.; Homer, M. E.; Champneys, A. R. Improving the Signal-to-Noise Ratio of High-Speed Contact Mode Atomic Force Microscopy. *Review of Scientific Instruments*. 2012. https://doi.org/10.1063/1.4747455.
(19) Picco, L. M.; Bozec, L.; Ulcinas, A.; Engledew, D. J.; Antognozzi, M.; Horton, M. A.; Miles, M. J. Breaking the Speed Limit with Atomic Force Microscopy. *Nanotechnology* **2007**, *18* (4), 44030. https://doi.org/10.1088/0957-4484/18/4/044030.
(20) Picco, L. M.; Dunton, P. G.; Ulcinas, A.; Engledew, D. J.; Hoshi, O.; Ushiki, T.; Miles, M. J. High-Speed AFM of Human Chromosomes in Liquid. *Nanotechnology* **2008**, *19* (38), 384018. https://doi.org/10.1088/0957-4484/19/38/384018.
(21) Pyne, A.; Marks, W.; M Picco, L.; G Dunton, P.; Ulcinas, A.; E Barbour, M.; B Jones, S.; Gimzewski, J.; J Miles, M. High-Speed Atomic Force Microscopy of Dental Enamel Dissolution in Citric Acid. *Arch. Histol. Cytol.* **2009**, *72* (4–5), 209–215. https://doi.org/JST.JSTAGE/aohc/72.209 [pii].
(22) Evans, C. T.; Payton, O.; Picco, L.; Allen, M. J. Visualisation of Microalgal-Viral Interactions by High-Speed Atomic Force Microscopy. *Front. Virol.* **2023**, *3*. https://doi.org/10.3389/fviro.2023.1111335.
(23) Ando, T.; Kodera, N.; Takai, E.; Maruyama, D.; Saito, K.; Toda, A. A High-Speed Atomic Force Microscope for Studying Biological Macromolecules. *Proc. Natl. Acad. Sci. U. S. A.* **2001**. https://doi.org/10.1073/pnas.211400898.
(24) Ando, T.; Uchihashi, T.; Kodera, N.; Yamamoto, D.; Taniguchi, M.; Miyagi, A.; Yamashita, H. High-Speed Atomic Force Microscopy for Observing Dynamic Biomolecular Processes. *J. Mol. Recognit.* **2007**, *20* (6), 448–458. https://doi.org/10.1002/jmr.843.
(25) Milhiet, P.-E.; Yamamoto, D.; Berthoumieu, O.; Dosset, P.; Grimellec, C. L.; Verdier, J.-M.; Marchal, S.; Ando, T. Deciphering the Structure, Growth and Assembly of Amyloid-Like Fibrils Using High-Speed Atomic Force Microscopy. *PLOS ONE* **2010**, *5* (10), e13240. https://doi.org/10.1371/journal.pone.0013240.
(26) Watanabe-Nakayama, T.; Tsuji, M.; Umeda, K.; Oguchi, T.; Konno, H.; Noguchi-Shinohara, M.; Kiuchi, Y.; Kodera, N.; Teplow, D. B.; Ono, K. Structural Dynamics of

Amyloid-β Protofibrils and Actions of Anti-Amyloid-β Antibodies as Observed by High-Speed Atomic Force Microscopy. *Nano Lett.* **2023**, *23* (13), 6259–6268. https://doi.org/10.1021/acs.nanolett.3c00187.

(27) Zhang, Y.; Tunuguntla, R. H.; Choi, P.-O.; Noy, A. Real-Time Dynamics of Carbon Nanotube Porins in Supported Lipid Membranes Visualized by High-Speed Atomic Force Microscopy. *Philos. Trans. R. Soc. B Biol. Sci.* **2017**, *372* (1726), 20160226. https://doi.org/10.1098/rstb.2016.0226.

(28) Feuillie, C.; Lambert, E.; Ewald, M.; Azouz, M.; Henry, S.; Marsaudon, S.; Cullin, C.; Lecomte, S.; Molinari, M. High Speed AFM and NanoInfrared Spectroscopy Investigation of Aβ1–42 Peptide Variants and Their Interaction With POPC/SM/Chol/GM1 Model Membranes. *Front. Mol. Biosci.* **2020**, *7*.

(29) Ewald, M.; Henry, S.; Lambert, E.; Feuillie, C.; Bobo, C.; Cullin, C.; Lecomte, S.; Molinari, M. High Speed Atomic Force Microscopy to Investigate the Interactions between Toxic $A\beta_{1\text{-}42}$ Peptides and Model Membranes in Real Time: Impact of the Membrane Composition. *Nanoscale* **2019**, *11* (15), 7229–7238. https://doi.org/10.1039/C8NR08714H.

(30) Robinson, M. The Interplay Between the Neuronal Plasma Membrane and Cell Signaling in Alzheimer's Disease. Doctoral Thesis, University of Waterloo, Waterloo, Ontario, Canada, 2023. https://uwspace.uwaterloo.ca/handle/10012/19196 (accessed 2023-07-04).

(31) Stine, W. B.; Jungbauer, L.; Yu, C.; LaDu, M. J. Preparing Synthetic Aβ in Different Aggregation States. *Methods Mol. Biol.* **2011**, *670*, 13–32. https://doi.org/10.1007/978-1-60761-744-0-2.

(32) Heaps, E.; Yacoot, A.; Dongmo, H.; Picco, L.; Payton, O. D.; Russell-Pavier, F.; Klapetek, P. Bringing Real-Time Traceability to High-Speed Atomic Force Microscopy. *Meas. Sci. Technol.* **2020**, *31* (7), 074005. https://doi.org/10.1088/1361-6501/ab7ca9.

(33) Davis, J. H.; Clair, J. J.; Juhasz, J. Phase Equilibria in DOPC / DPPC-d 62 / Cholesterol Mixtures. *Biophysj* **2009**, *96* (2), 521–539. https://doi.org/10.1016/j.bpj.2008.09.042.

(34) Robinson, M.; Filice, C. T.; McRae, D. M.; Leonenko, Z. Atomic Force Microscopy and Other Scanning Probe Microscopy Methods to Study Nanoscale Domains in Model Lipid Membranes. *Adv. Phys. X* **2023**, *8* (1), 2197623. https://doi.org/10.1080/23746149.2023.2197623.

(35) Lee, J.; Kim, Y. H.; Arce, F.; Gillman, A. L.; Jang, H.; Kagan, B. L.; Nussinov, R.; Yang, J.; Lal, R. Amyloid β Ion Channels in a Membrane Comprising Brain Total Lipid Extracts. *ACS Chem. Neurosci.* **2017**, *8* (6), 1348–1357. https://doi.org/10.1021/acschemneuro.7b00006.

(36) Bode, D. C.; Freeley, M.; Nield, J.; Palma, M.; Viles, J. H. Amyloid-β Oligomers Have a Profound Detergent-like Effect on Lipid Membrane Bilayers, Imaged by Atomic Force and Electron Microscopy. *J. Biol. Chem.* **2019**, *294* (19), 7566–7572. https://doi.org/10.1074/jbc.AC118.007195.

(37) Robinson, M.; Lee, B. Y.; Hane, F. T. Recent Progress in Alzheimer's Disease Research Part 2 - Genetics and Epidemiology. *J. Alzheimers Dis.* **2017**, *57* (2), 317–330. https://doi.org/10.3233/JAD-161149.

(38) Cecchi, C.; Nichino, D.; Zampagni, M.; Bernacchioni, C.; Evangelisti, E.; Pensalfini, A.; Liguri, G.; Gliozzi, A.; Stefani, M.; Relini, A. A Protective Role for Lipid Raft Cholesterol against Amyloid-Induced Membrane Damage in Human Neuroblastoma Cells.

Biochim. Biophys. Acta **2009**, *1788* (10), 2204–2216. https://doi.org/10.1016/j.bbamem.2009.07.019.